

Development of Neutron Shields for Gamma-ray Detectors

J. Hong, C. J. Hailey, and W. W. Craig

Columbia Astrophysics Laboratory, Columbia University 538 W.120th St., NY, NY 10027, USA

ABSTRACT

The importance of shields for suppressing neutron-induced background in new classes of γ -ray detectors such as CZT has been emphasized for a variety of reasons. These include high cross-sections for neutron interactions in detector materials and inefficient vetoing of neutrons in conventional active shields. We previously demonstrated through Monte-Carlo simulations how our new approach, supershields, is superior to the monolithic, biatomic neutron shields which have been developed in the past.

Here we show the construction of several prototype models for supershields using B and H. We verify the performance of these supershields through lab experiments using radioactive sources and monoenergetic neutron beam at the Radiological Research Accelerator Facility(RARAF*), and compare the results with monolithic neutron shields. We also discuss the implications of this experiment for designs of supershields in general.

Keywords: neutrons, background, supershields

1. INTRODUCTION

In balloon-borne or satellite-based γ -ray telescopes, sensitivity improvement is usually achieved by increasing detector size or introducing active shields to veto external background. These methods have reached the limit due to mass constraint on the payload and because of secondary particle production from interactions with cosmic-rays in the spacecraft(S/C) and shields.

The neutron-induced background(n-background), which has non-prompt components as well as prompt components, is from atmospheric albedo neutrons and neutrons generated by secondary interactions in the S/C. Except for some of n-background, conventional active shields are very inefficient in vetoing it, and increasing the size of the shields does not help because of the secondary particle production. This is why n-background would be dominant or a considerable portion of total background in new classes of detectors like CZT with a thick active shield like BGO or traditional alkali halide.²

There was an investigation of neutron shields for γ -ray detectors a decade ago.^{3,4} Recently we introduced the *supershield* to approach this problem. We also developed neutron source functions for accurate modeling.⁵⁻⁷ We demonstrated supershields are superior to conventional neutron shields through Monte Carlo simulation. Supershields are designed to shield n-background as well as other external background. The standard configuration consists of 3 separate layers, i.e. active shield, absorber, and moderator.

Supershields are distinguished from conventional neutron shields by novel arrangements and proper choices of shielding materials. Having separate layers of absorber and moderator not only increases the efficiency for shielding neutrons but also suppress epithermal neutrons generated in the shield, which were one of the major problems in the previous attempts to develop neutron shields.

Previously we also discussed glass microspheres,⁸ which make it practical to have gaseous forms of shielding materials like ^3He and H_2 . Specially in the case of ^3He , despite its high interaction cross sections with neutrons, it was considered impossible to use in space applications simply because it was unavailable in a safe and high dense state to be effective for shielding. The perfect symmetry in the shape of microspheres allows them to sustain very high pressures. They can hold up to ~ 200 atm of gas.

Send correspondence to J. Hong

J. Hong: E-mail: flame@cuphy3.phys.columbia.edu

*Radiological Research Accelerator Facility at Nevis Laboratories, Columbia University, P.O. Box 21, Irvington, NY 10533¹

In this paper we discuss prototype models for supershields using B and H which are effective moderators and absorbers. We verify the performance of these supershields through lab experiments using radioactive sources and monoenergetic neutron beams at RARAF.

Using ^3He and H_2 proportional counters, we measure high energy neutrons and low energy neutrons transmitted through the shields. We briefly summarize neutron detector interactions.

Here we focus on identifying differences in various shields defined in terms of neutron transport through the shields. With Monte-Carlo simulation, we can design optimal configurations of supershields for specific telescopes. This experiment will also be a guide in constructing supershields of other materials, such as gas microspheres.

In order to be useful in applications, shields should not only be good at absorbing neutrons but also should not produce many secondary particles from the interactions with cosmic-rays. This is one of the reasons why low atomic weight materials are preferred to high weight ones like Cd as shielding materials, even though Cd has huge neutron interaction cross sections. This is a first experimental step in a series of lab experiments to develop effective neutron shields, which will include tests on secondary particle productions in the shields.

2. EXPERIMENTAL SETUP

To measure neutron transport through shields, one has to identify the intensity and the spectrum of incoming and outgoing neutrons. We utilize RARAF to get monoenergetic neutron beams onto shields, and use two neutron detectors, ^3He and H_2 gas proportional counters (GPC), to identify high and low energy neutrons. We also use a NaI crystal detector to measure γ -ray background generated in the shields and a tissue equivalent ionization chamber (IC) to monitor the variation of neutron beam intensity.

2.1. Neutron Source

RARAF provides a source of monoenergetic neutrons designed and operated specifically for studies in radiation biology, dosimetry, and microdosimetry. Neutron spectroscopy often adapts the time of flight (TOF) measurement technique by using pulsed neutron beams in order to get a precise energy spectrum of neutrons. Unfortunately, RARAF is not equipped for TOF measurements, but its ability to generate monoenergetic neutron beams makes it easy to calibrate our neutron detectors and also to do neutron spectroscopy.

The primary beams (H, D, He ions) are directly produced by the RARAF Van de Graaff accelerator. All of the accelerated beams are available for radiological physics, and the intense hydrogen and deuterium beams are used to produce secondary beams of either neutrons or ultrasoft x rays. Neutrons are generated at RARAF using nuclear reactions in thin targets and thus are essentially monoenergetic, in contrast to neutrons generated by reactors or by high energy deuterons bombarding beryllium targets. RARAF's neutron production targets are hydrogen isotopes absorbed into thin titanium coatings on water-cooled copper backings. Monoenergetic neutrons with energies from 100 keV to 14 MeV are available as shown in table 1.

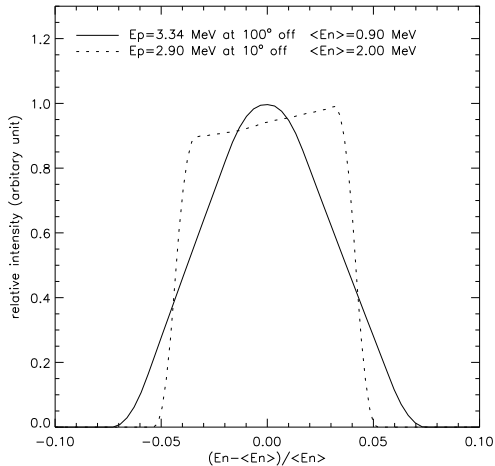
Room	Targets & Interactions	Q-value	Neutron Energies	Energy Resolution
SV cave	$^7\text{Li}(p,n)^7\text{Be}$	-1.65 MeV	$\sim 100 \text{ keV} - 400 \text{ keV}$	$\sim 10 - 20 \%$
SH cave	$\text{T}(p,n)^3\text{He}$	-764 keV	$\sim 400 \text{ keV} - 3 \text{ MeV}$	$\sim 10 - 15 \%$
SH cave	$\text{D}(d,n)^3\text{He}$	3.27 MeV	$\sim 3 - 6 \text{ MeV}$	$\sim 2 - 6 \%$
SH cave	$\text{T}(d,n)^4\text{He}$	17.6 MeV	$\sim 14 - 20 \text{ MeV}$	1 - 4 %
$^{241}\text{Am}/\text{Be}$	$^9\text{Be}(\alpha,n)^{12}\text{C}$	5.71 MeV	up to 10 MeV	

Table 1. Neutron beams at RARAF and $^{241}\text{Am}/\text{Be}$ radioactive neutron source

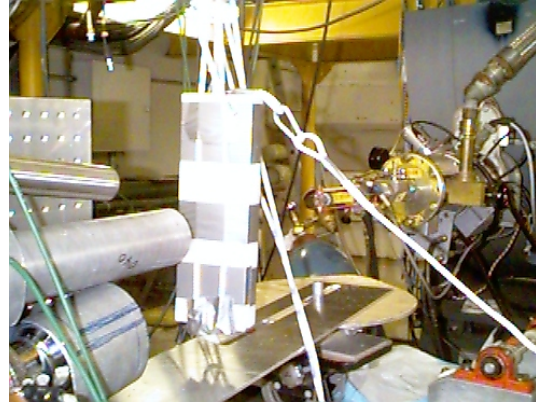
In this experiment, we used a Ti+T target (Ti thickness= $2.224 \text{ mg}/\text{cm}^2$, T/Ti ratio=2.10) to get neutrons from 500 keV to 3 MeV. Neutrons emerge isotropically from the target, and their energies are determined by the proton energy and the angle between primary proton beam and output neutron momentum direction.⁹ In order to minimize energy spread, irradiations are conducted at 100 degrees from the primary beam direction for the neutrons from 500 keV to 1 MeV, and at 10 degrees for neutrons above 1 MeV. Figure 1a shows the neutron energy distributions in a 2'' window at 30'' away from the target. This spread is due mainly to the finite thickness of the target and window

size. In figure 1b, one can see the Ti target, IC and 3 detectors which are set at 10° off from the primary beam direction.

We use a radioactive neutron source $^{241}\text{Am}/\text{Be}$ to calibrate the ^3He GPC.¹⁰ The neutrons emerges with energies up to 10 MeV ($\sim 23\%$ below 1 MeV with mean energy 400 keV). The source strength is not high enough to (50 mCi) to measure the high energy part of the spectrum in the ^3He GPC, but the epithermal peak[†] is well detected. In the case of H_2 GPC, due to its peculiar response function, it is very hard to do spectroscopy on the radioactive source directly without knowing the detector response matrix.¹¹



(a) Energy distribution of neutrons passing through 2'' window at 30'' from the target, which is roughly the center of ^3He GPC. The spread is mainly due to the thickness of the target and the size of the window. Because of the size and cylindrical shape of GPC, the spectrum of neutrons entering the detector will be slightly different from the plot above. (E_p : proton energy, E_n : neutron energy)



(b) A view inside SH cave at RARAF showing the Ti target with beam pipe in the middle (right above the disk-shaped table), 3 detectors pointing at the target at the left bottom corner (H_2 , ^3He GPC, and NaI detector from top to bottom, 10° offset from the primary beam direction), and a 1.25'' thick polyethylene shield between the Ti target and the detectors. ^3He GPC is wrapped with 0.040'' Cd sheets. The shields are brought in remotely by motors. To cover all three detectors, they are about 12'' tall, and 4'' wide. (Table 3)

Figure 1. Neutron source characteristics and a view inside SH cave at RARAF

2.2. Neutron Detectors

Because the cross section for neutron interactions with most materials is a strong function of neutron energy, rather different techniques have been developed for neutron detection in different energy regions.¹²

Low energy (~ 1 eV) neutron spectroscopy can be done in a crystal spectrometer or mechanical monochromator. In general, interactions to detect neutrons involves reaction Q 's of order a few MeV. Commonly available proportional counter or scintillators cannot spectroscopically resolve few eV neutron energies. They simply serve as counters. The popular materials for detecting low energy neutrons are ^{10}B , ^3He , and ^6Li due to their high cross sections. We adapted a ^3He GPC using the interaction $^3\text{He}(n,p)\text{T}$, which is the inverse of the neutron production interaction at RARAF. (Table 2.)

This type of GPC is effective in the presence of γ -ray background due to the low density of the detecting material compared to crystal or plastic scintillators. X-ray or soft γ -ray GPC tend to have very thin windows for photon transmission, but GPC for neutron detection can have a relatively thick wall which can block soft γ -rays. The ^3He GPC has only a small probability for stopping γ -rays and γ -rays generally deposit only part of their energy.

However the ^3He is subject to the so-called "wall effect",¹³ which is incomplete pulse collection caused by collisions between the detector wall and the secondary particles from neutron interactions. Because the pulse rise time from each event depends on how the particles lose their energies in the detector, analysis of pulse rise time gives very useful information for distinguishing different type of events in the detector.^{14,15} For instance, γ -ray events tend to have longer rise times than other charged particle events due to longer tracks of energy deposition in the detector.

[†]The meaning of epithermal neutrons varies. We define them as neutrons, which have been moderated into the thermal or low energy

detector	^3He gas proportional counter	H_2 gas proportional counter
Interactions	$^3\text{He}(n,p)\text{T}$	$\text{H}(n,n)\text{H}$
Components (pressure, atm)	$\text{CO}_2:\text{Ar}:^3\text{He}$ (91.2:1520.0:2948.8)	$\text{N}_2:\text{CH}_4:\text{H}_2$ (100:100:3040)
Dimension ^a	$1.45'' \times 8.2''$	$2'' \times 9.75''$
resolution	$\lesssim 10\%$ at 1 MeV	$\lesssim 10\%$ at 1 MeV
efficiency ^b	$\sim 100\%$ at $E < 1$ eV	$\sim 1 - 2\%$ at $E = 1$ MeV
function ^c	Counting low energy neutrons Spectroscopy on neutron from 1 to 3 MeV	Spectroscopy on neutron from 300 keV to 2 MeV

^aCylindrical shape, diameter \times length

^bWhen neutron enters through one of end cap in the GPC and its path is parallel to the axis of GPC cylinder.

^cFor higher energy neutrons, one needs to change the pressure of detectors.

Table 2. Properties of the Detectors

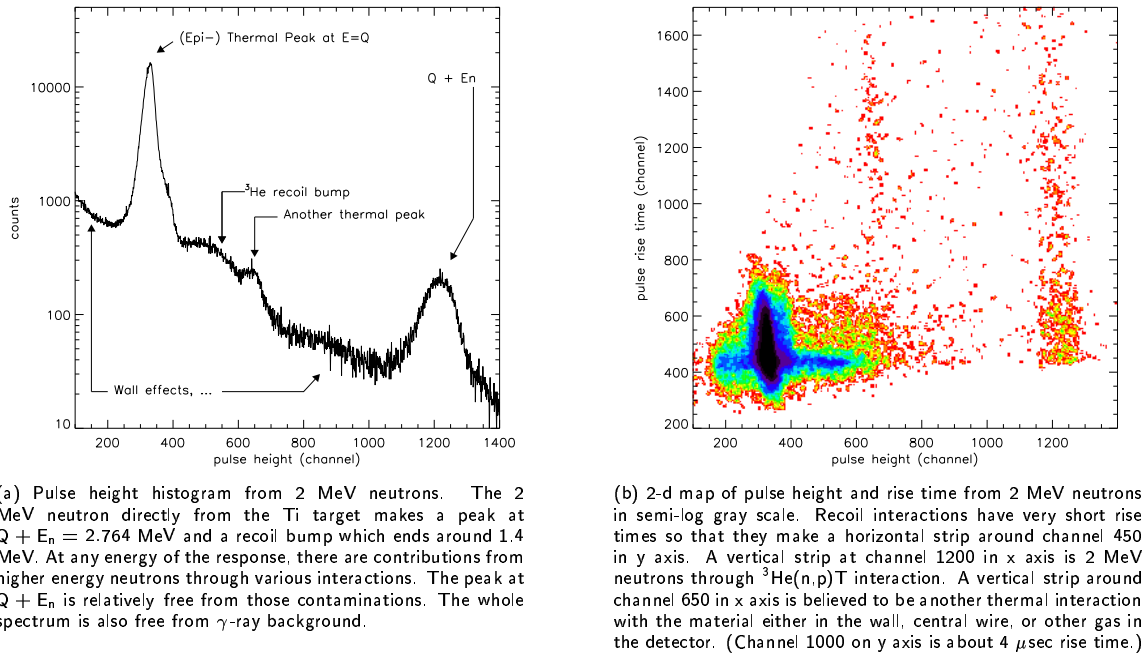


Figure 2. ^3He GPC response

With proper use of pulse rise time analysis, one can also use ^3He GPC as a high energy neutron spectroscopy detector from 100 keV to 8 MeV, even though it is relatively inefficient.¹⁴ The pulse height histogram of ^3He GPC from 2 MeV monoenergetic neutrons is shown in figure 2. Since the Q of the reaction is 764 keV, 2 MeV neutrons make a peak around $0.764+2$ MeV. There is a peak at 764 keV from ambient epithermal neutrons and there is also a bump from the recoil interaction $^3\text{He}(n,n)^3\text{He}$, which ends around $\sim 75\%$ of the original neutron energy. The 2-dim map of pulse rise time and pulse height in figure 2b shows how one can use this detector as a spectrometer above 1 MeV. A simple cut on events whose pulse rise times are less than $4\mu\text{sec}$ would remove events in a major thermal peak and from recoil interactions.

In high energy neutron spectroscopy (~ 100 keV – 10 MeV), recoil interactions(elastic scattering) are commonly region by the shield environment, which deposit the same energy (the reaction Q value) in the detector. The resulting peak is usually called the epithermal peak.

used to detect neutrons. Other than TOF measurements, a good way to achieve high energy resolution is *proton recoil telescopes* using proton-neutron elastic scattering.¹² However it is very inefficient in detecting neutrons and requires a fair amount space just for the detection system. We used one of the simplest detectors, H₂ GPC, which also uses H recoil interactions.

H recoil neutron detectors have a response function different from other neutron or γ -ray detectors. Since incident neutrons can lose any portion of their energies through elastic scatterings, the theoretical response to monoenergetic neutrons is flat from zero to the incident neutron energy. In addition to this, wall effect, finite energy resolution and other competing interactions (with other materials in the detectors) modify the neutron spectrum as well. To do accurate spectroscopy, one has to have unfolding procedures for the response.¹¹

Figure 3 shows the responses of an H₂ GPC for 500 and 900 keV neutrons. For monoenergetic neutrons, the location of the shoulder in the response correlates with the incident neutron energy.

We also adapt an NaI crystal detector to estimate γ -ray background. Neutron beams from the target are not collimated, so that once they are turned on, there are epithermal neutrons generated around the room. These neutrons quickly activate the NaI γ -ray detector, so that it is very hard to localize γ -ray emissions from neutron interactions in the shields. It will be used to measure γ -ray background inside the shields when complete 3-D models of supershields are available. With collimated neutron beams at particular energies, this γ -ray detector also gives very useful information.

In order to keep track of the beam intensity, a tissue equivalent ionization chamber(IC) was introduced. Even though it responds to every type of radiation in the room, it gives a signal roughly proportional to the intensity of the neutron beams from the target.

The cylinder axis of ³He, H₂ GPC an NaI crystal detector are set to point to the Ti target in order to increase neutron path length in the detectors. (Figure 1) The location of the detectors is about 30'' from the Ti target. This is roughly in the middle between the Ti target and the wall of the cave, so that we can minimize energy dispersion at the detection point (the further from the Ti target, the smaller the dispersion), and also reduce epithermal neutrons from the wall (the closer to the Ti target, the smaller the epithermal n-backgrounds).

2.3. Electronics

In order to get the pulse rise time and the pulse height from each event, we use a delay line amplifier with a pulse shape analyzer and subsequent electronics. Each signal from the detector goes through 2 different electronic channels, one for the pulse height and the other for the pulse rise time. Figure 4 shows the basic electronics for one detector. The IC updates the fluctuations of the neutron beam intensity at 10 Hz frequency, which is used to normalize the neutron counts.

2.4. Shields

The standard configuration of supershields⁵ consists of 3 layers, i.e. absorber, moderator, and active shield. Since here we are interested in the neutron transportation through shields, we tested only moderators and absorbers.

In order to find the difference in shielding performance coming from the arrangements of shielding materials, we used absorbers and moderators containing only B and H in this experiments.(section 3) We used high-density polyethylene with ¹⁰B powder as a model of a standard configuration of supershield, and natural B doped polyethylene

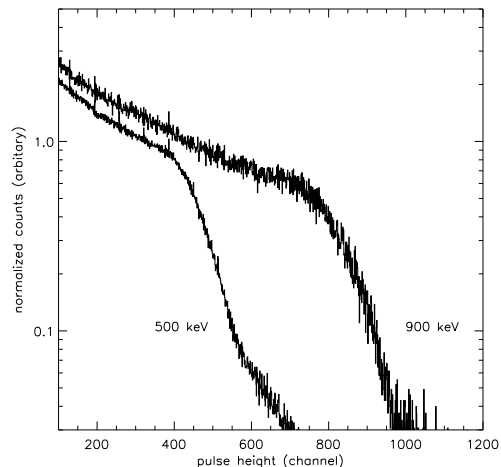


Figure 3. Response of H₂ GPC from 500 and 900 keV neutrons, The location of the shoulder in the response roughly indicates the energy of incident neutrons. For non-monochromatic neutrons, one has to rely on unfolding procedures to find the input spectrum.

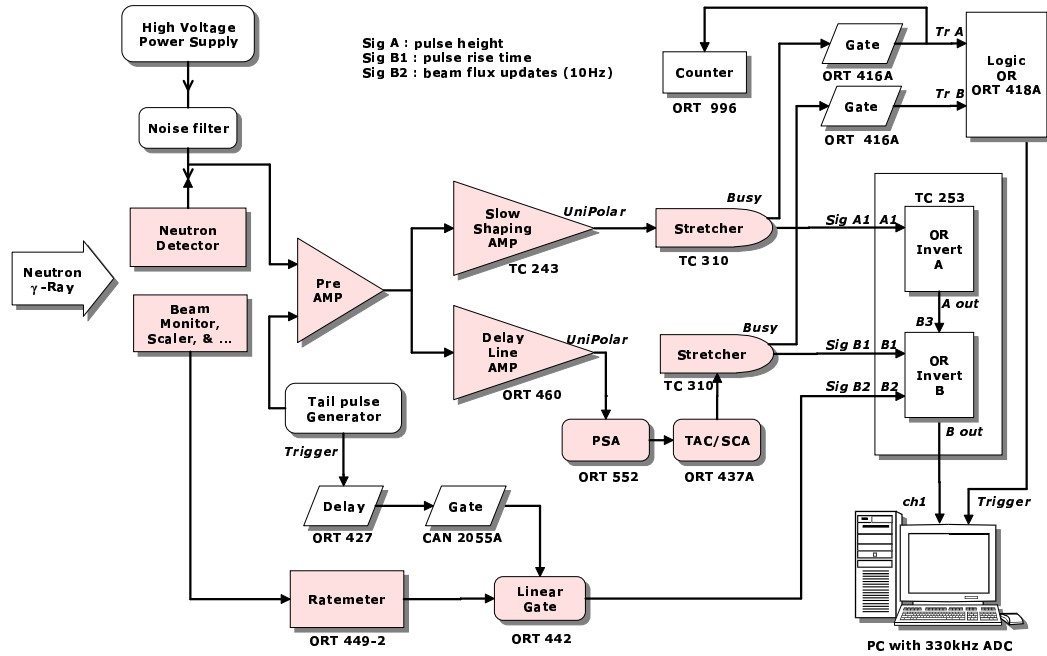


Figure 4. Electronics Setup for neutron detector. Combinations of delay line amplifier, pulse shape analyzer(PSA), and time-to-analog convertor(TAC) are used for pulse rise time measurements.

as a model for a conventional neutron shield. We also tested ^{10}B and polyethylene separately in order to characterize the role of each material. Table 3 shows the properties of shielding materials used, and the last column lists 4 specific shield configurations which are analyzed later in this paper.

In order to reduce the ambient thermal neutrons and subsequently increase the efficiency for detecting only moderated neutrons from the shield, we wrapped the ^3He GPC with $0.040''$ Cd sheet except for the opening to the Ti target.

The shields are placed between the detectors and the Ti target remotely by using motors. The $12''$ tall, $4''$ wide shields cover the neutron path from the Ti target to all 3 detectors. The geometrical path lengths of the neutrons through the shield are slightly different from detector to detector, depending on the locations of the detectors. (See figure 1b)

Since the shields subtend more solid angle from the Ti target than the detectors do, the energy of neutrons entering the shields will be more spread than those entering detectors when there is no shield.

As mentioned earlier, the true performance of shields should be determined by suppressing neutron interactions in the detectors and also by secondary particle generation in the shields. In the case of ^{10}B , $480\text{ keV } \gamma\text{-rays}$ are generated through the neutron absorption interaction $^{10}\text{B}(n,\gamma)^{11}\text{B}$. If one is interested in detecting $511\text{ keV } \gamma\text{-ray}$ line from astrophysical sources, adapting neutron shields with ^{10}B would be inappropriate. In that case, neutron shields with ^3He or other material would be preferred since ^3He does not have a $\gamma\text{-ray}$ associated with the interaction $^3\text{He}(n,p)\text{T}$, and the decay products do not generate important background. For experimental verification of the supershield concept, it is easier to work with the more readily available Boron.

Material	Element analysis (mg/cc)	one unit dimension ^a	configurations	configurations analyzed
natural B doped Polyethylene ^b	C:B:H:(Si,O,Fe,Al,Mn) 705:357:102:26	12.1'' × 4.25'' × 2.1'' (used in stacks of 1, 2, or 3 units)	Serve as prototype of Conventional shield	• BdP : 2.1'' thick
Pure ¹⁰ B powder	¹⁰ B 900	7.0'' × 4.0'' × 0.0787'' or 7.0'' × 4.0'' × 0.354''	Separately or With polyethylene	• B+P(I) : 1.25'' thick Poly + 0.354'' ¹⁰ B • B+P(II) : 1.25'' thick Poly + 0.0787'' ¹⁰ B
High density Polyethylene	C:H 765:135	12.0'' × 4.0'' × 0.25'' (used in stacks of 2, 5, and 11 units)	Separately or With ¹⁰ B powder	• P : just 1.25'' thick Polyethylene
Cd	8650	0.040''	For ³ He detector	

^aheight × width × thickness. The thickness of the shields are roughly equivalent to the geometrical path lengths of the neutrons through the shield. The number in () is the number of units used at a time. Having 2 units is equivalent to doubling the thickness of the unit.

^bNatural boron contains 19.9% of ¹⁰B.

Table 3. Shielding Materials. All of them are based on B or H except for Cd sheet which is used to characterize the thermal neutrons. We analyzed data from 4 different shield configurations listed in the last column in this paper.

2.5. Measurement

There were 4 sets of measurements as shown in table 4. The first set was mainly to verify the detector system and to get the basic response functions for H₂ GPC. These response functions, along with those at other energies, will be used for a detail analysis. The second and third sets were for testing shielding performance in various configurations. The fourth set was for a few complementary measurements. This includes measurements of different detector locations and orientations and of Cd as a shield to characterize thermal neutrons entering detectors from the direction of the Ti target. For 900 keV neutrons in the third and 2 MeV neutrons in the fourth measurement, 9 and 6 different shield configurations were tested respectively. For other cases we tested 2 or 3 different configurations. Before and after the measurements of each shield configuration, we also took data from the neutron beams without any shield for comparison and for monitoring neutron beam fluctuations.

Neutron Energies (MeV)	Shields Configuration	Detectors	Purpose
0.6, 0.7, 0.8, 0.9, 1.0	BdP	³ He, H ₂ , NaI	Detector calibrations
0.5, 0.7, 1.0, 2.0	BdP, B+P, P	³ He, H ₂ , NaI	Shield performance
0.9, 2.0, 2.8	BdP, B+P, B, P	³ He, H ₂ , NaI, IC	Shield performance
0.1, 0.8, 0.9, 2.0	BdP, B+P, P, Cd	³ He, H ₂ , IC	Shield performance

Table 4. Experiment configurations and Energy

3. EXPERIMENTAL GOAL

While a long term goal of this experiment is the construction of good supershields for a given γ -ray detector, a short term goal would be the verification of the simulation codes COG¹⁶ or HETC¹⁷ which are used to design and optimize shield configurations.

One of the interesting implications from the simulations in a previous paper⁶ was the strong difference in shielding performance due to differing arrangements of shielding materials. To focus on this matter and verify simulation results, we tested absorbers and moderators utilizing only B and H. Two extreme cases of putting 2 materials together would be either having absorber and moderator in the same matrix, which was used by previous researchers or having separate absorber and moderator layers, which is the standard configuration in a supershield.

The choice of detailed configuration and shielding materials for a specific telescope will be decided by the type of the γ ray detector and the background generated by the S/C. The optimal design could be different from the cases tested – we are attempting to validate the basic concept. Tests on these 2 extreme arrangements will be a basis for understanding the physics of more complicated configurations.

Lately it has suggested that high energy neutrons are the dominant neutron background in S/C⁶ in some balloon telescopes.^{2,18} Both conventional neutron shields and supershields are efficient in moderating high energy neutrons, but they show marked differences in absorption of moderated neutrons.

Figure 5 compares the output neutron spectrum from supershield and conventional neutron shield with 2 MeV monoenergetic neutron input in a 1-dim simulation. For a fair comparison, each configuration has the same amount of ^{10}B and H (\blacktriangle , \circ in the figure). However they show dramatic differences in the low energy part of the spectrum. If a γ -ray detector under consideration has high interaction cross section with neutrons whose energies are less than 1 keV, having a shield in a wrong configuration would be problematic.

In a conventional neutron shield, moderation always leaves low energy neutrons, while a supershield suppresses the low energy neutrons. as shown in figure 5. Also with the same amount of material, the supershield is more efficient in removing the original high energy neutrons.

The results are slightly different from the lab experiments since this simulation is done in a perfect 1-dim configuration. However the general tendency will be the same.

The task in the experiments is to identify moderated neutrons and characterize their flux and energies.

Getting a precise neutron spectrum from the GPC requires use of histogram unfolding procedures, which should include energy dependent wall effect, finite resolution, energy dependent efficiency, recoil effect, and interactions with other nuclei in the gas. This should also be combined with complete 3-d simulations in order to understand the details of physics. However, here we extract semi-quantitative results directly from the pulse height histograms without detailed analysis. More complete results will be presented elsewhere.

4. RESULTS AND DISCUSSION

Due to the short period of time since acquiring this data, we only perform a crude qualitative analysis here. A more detailed analysis will be presented elsewhere.

The ^3He GPC gives extensive information on the neutron spectrum from thermal to high energy. Figure 6, shows the pulse height histograms of ^3He GPC for 3 different shield configurations. Except for the highest energy region, the counts in any energy channel(pulse height channel) contain the contributions from higher energy neutrons through various interactions, so that the shape of the pulse height histogram is quite different from the shape of the original neutron spectrum. Yet each shield provides a unique characteristic spectrum from which the incident neutron spectrum can be extracted.

In the case of the neutrons in the input energy region (IE), (around 2 MeV for figure 6), the change of the pulse height histogram directly indicates the changes of the neutron spectrum in that energy region, since the IE region is free from contributions from the neutrons of other energies.

In order to get an idea of the spectrum changes at lower energies, first we remove contributions from neutrons of the IE region in the histogram h_{s_i} with a shield s_i ($=$ BdP, B+P, or P in the figure 6) by forming

$$\Delta h_{s_i} = (h_{s_i} - \frac{C_{s_i}^{ie}}{C_o^{ie}} h_o)$$

where h_o is the histogram with no shield and $C_{s_i}^{ie}(C_o^{ie})$ are the counts in IE region with the shield (no-shield).

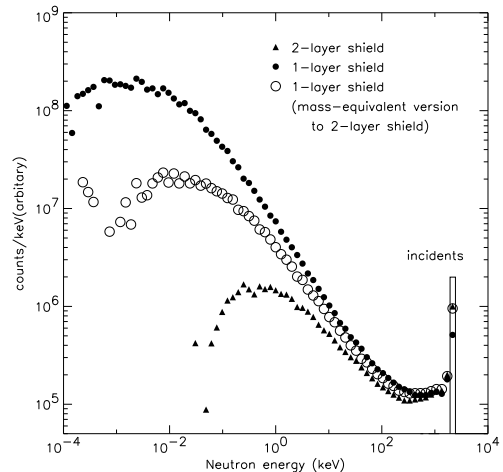


Figure 5. Differential neutron spectra from shields with different arrangements of the shield materials. Input spectrum is 2 MeV monoenergetic neutrons. \bullet has the same amount of ^{10}B and H as (BdP) and \blacktriangle as (B+P(l)).(Table 3.) When they have equivalent amount of mass, the difference becomes outstanding at low energies.

Δh_{s_i} still has huge contributions from ambient epithermal neutrons. If we assume those contributions are independent of shield (true to first order[†]), the difference in Δh_{s_i} for each shield compared to that of another shield will give an idea of neutron spectrum changes from each shield. In order to show this effectively, we form the quantity

$$\Delta h'_{s_i} = \Delta h_{s_i} / h_o C$$

assuming h_o gives roughly the same histogram at low energies as the ambient epithermal neutrons. (C is a normalization constant which is the same for any shield.)

$\Delta h'_s$ for each shield is shown on the bottom of figure 6. In this plot, one can see the difference at low energies for different shields. In the case of P, there is a huge enhancement next to the main thermal peak (channel 300-400), which demonstrates an increased number of neutrons from a few keV up to a few 100 keV. This is mainly due to lower neutron absorption. Also there is an excess of thermal neutrons in BdP compared to B+P. The peak around channel 650 is due to another interaction for thermal neutrons.

Now in order to obtain an overview of spectrum changes, we divide the neutron spectrum into 4 energy sections, thermal (TE), low energy (LE: > TE, < 100 keV), high energy (HE: ~ 100 keV - E_n), and incident neutron beam energy region (IE: around E_n) and then trace the changes of neutrons in each section. (E_n : the energy of neutron from the Ti target)

Neutrons in the IE region can be defined as the number of counts in the full width half maximum (FWHM) of the peak at $Q + E_n$ from the ^3He GPC response.

The changes in the HE region are calculated by the counts in the H_2 GPC pulse height histogram above the channel which roughly equals 100 keV, after the subtraction of the contribution of the IE neutrons. If g is the histogram from H_2 GPC, the number of neutrons in the HE region is given by

$$\sum_{>100\text{keV}} \Delta g_s = \sum_{>100\text{keV}} (g_s - g_o \frac{C_s^{ie}}{C_o^{ie}})$$

Since a neutron can deposit any portion of its energy in the H_2 GPC, this is only an approximation of the number of neutrons from 100 keV to E_n , but the proportionality is valid.

For the changes in the TE region, the sum of $\Delta h'_{s_i}$ from zero to the thermal peak in the ^3He GPC histogram would be a good indicator. However the recoil interactions start giving substantial contributions at low energies. We chose the sum $\Delta h'_{s_i}$ within the FWHM of the main thermal peak for TE neutrons. For the changes in the LE region, we use the sum of $\Delta h'_s$ above the FWHM of the thermal peak and below the channel which is equivalent to $Q+100$ keV. Figure 6 shows the region of TE, LE, and IE. The comparison for the TE and LE region is meaningful only in a relative sense.

[†]There are shield dependent contributions like *scattering-into-shield* events, which means some high energy neutrons not directly from the Ti target entered the shields and moderated, bounced back to the detector and were counted. We expect that this number is small since the angle coverage of the detector is quite small.

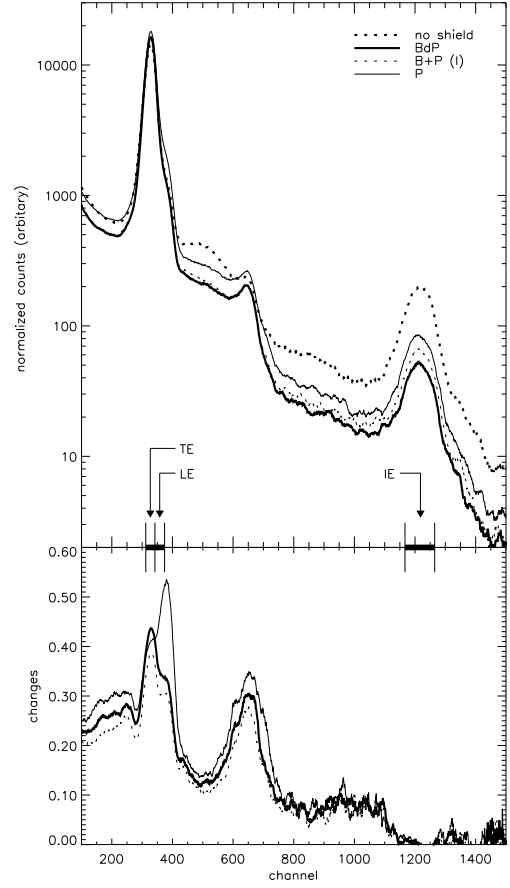
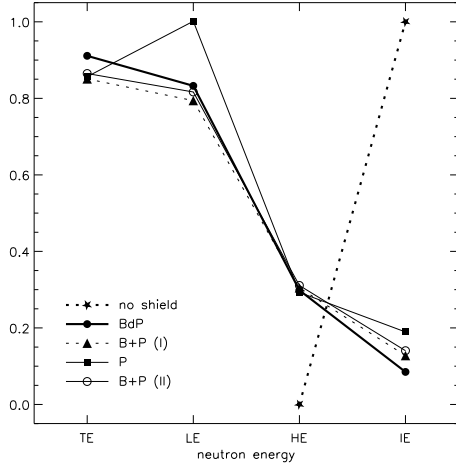
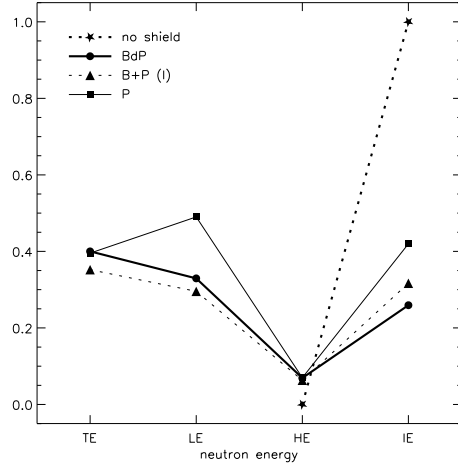


Figure 6. Comparison of ^3He GPC response from different shields and $\Delta h'_s$ plots. ^3He GPC response is used to trace the changes in neutron spectrum in TE, LE, IE section as marked in the plot. The peak around channel 650 is due to another thermal interaction, which just tells the changes of thermal neutrons.



(a) Changes of neutrons at each section normalized to the number of the neutrons in the IE region when no shield is present. Incident neutrons are 900 keV.



(b) The same plot as (2) with 2 MeV neutrons.

Figure 7. Changes of neutrons at each section. There are more neutrons in the TE and LE regions for BdP and P compared to B+P. Especially at 900 keV B+P(II) shows better performance suppressing LE and TE neutrons compared to BdP, even though it has a smaller amount of ^{10}B . As explained in the text, the number of neutrons in the TE and LE sections has meaning only in a relative sense.

Figure 7 summarizes the performance of the shield configurations for 900 keV and 2 MeV neutrons. They show the exact same trends determined from simple 1-d simulations. One can easily notice that there are substantial changes from P to BdP and B+P due to different neutron absorption. Lack of absorber leads to large enhancements in TE and LE neutrons. For BdP and B+P(II) with 900 keV input neutrons, even though the amount of ^{10}B in B+P(II) is smaller than in BdP, there is less increase of TE and LE neutrons. BdP shows less neutrons in the LE region than P, but the results in the TE region are comparable. This gives us an indication of how moderated the original neutrons are since both configurations have different amounts of H in the shields. For HE neutrons, all 3 shields show roughly the same performance, and for IE neutrons, BdP shows better performance due to the excess of H and C over the other shield configuration.

5. CONCLUSION AND FUTURE WORK

We have built a simple 1-dim supershield and measured its performance. Using the same materials, we focused on identifying the difference in shielding performance coming from different arrangements of shielding materials. As shown in figure 7, the difference is quite noticeable even with this simple analysis and the result agrees with the prediction of simulations.

In order to quantify the results, the complete analysis of data using the detailed response functions for the detectors and with 3-d simulations of the experiment implementing details of experiments is underway.

Future work will emphasize several directions. In terms of shield construction, 3-dim shield configurations which can hold a γ -ray detector inside will be evaluated, along with development of proto-type supershields using other materials like ^3He filled microspheres. For the neutron transport analysis, tests will involve a wider range of neutron energies, ~ 1 keV to 100 MeV. The region from 10 to 100 MeV will be interesting due to the lack of well established lab experiments in that region.

For the modeling, we will develop complete 3-dimensional simulations of realistic space experiments using our coupled neutron-photon transport and particle production codes in order to estimate the potential performance improvement in the experiments from supershields.

ACKNOWLEDGMENTS

We wish to thank Professor David J. Brenner of Columbia University for permitting us to use RARAF and Stephen A. Marino for technical assistance. We also thank Irwin Rochwarger for technical advices on electronics. This work was supported by the NASA Innovative Research Program under grant NAGW-4818. This work is contribution number 662 of the Columbia Astrophysics Laboratory.

REFERENCES

1. "Raraf user's guide," 1997.
2. F. Harrison et al *in preparation* .
3. C.S. Dyer, P.R. Truscott, C. Comber and N.D.A. Hammond *IEEE Trans. Nucl. Sci.* **NS-34**, No. 6, p. 1530, 1987.
4. C.S. Dyer, P.R. Truscott, A.J. Sims, C. Comber and N.D.A. Hammond *IEEE Trans. Nucl. Sci.* **NS-35**, No. 6, p. 1407, 1988.
5. C.J. Hailey and F.A. Harrison *Nucl. Instr. and Meth.* **A365**, p. 518, 1995.
6. J. Hong and C. J. Hailey. *Journal:Proc SPIE* **2806**, p. 449, 1996.
7. J. Hong and C. Hailey *in preparation* .
8. C.D. Hendricks and J.L. Dressler *Lawrence Livermore National Laboratory Report UCRL-50021-76*, 1976.
9. H. Liskien and A. Paulen *Nuclear Data Tables* **11**, pp. 569–619, 1973.
10. E. A. Lorch *Int. J. Appl. Radiat. Isotopes* **24**, p. 588, 1973.
11. V. V. Verbinski and R. Giovannini *Nucl. Instr. Meth.* **114**, p. 205, 1974.
12. G. F. Knoll, John Wiley & Sons, Inc., 1979.
13. Z. F. S. Shalev and J. M. Cuttler *Nucl. Instr. Meth.* **71**, p. 292, 1969.
14. A. Sayres and M. Coppola *Rev. Sci. Inst.* , p. 431, 1964.
15. S. Izumi and Y. Murata *Nucl. Instr. Meth.* **94**, p. 141, 1971.
16. T.P. Wilcox Jr. and E.M. Lent *Lawrence Livermore National Laboratory Report M-221-1,4*, 1989.
17. T. A. Gabriel, J. E. Brau, B. L. Bishop **ORNL/TM 11060**, 1989.
18. J. E. N. et al *Nucl. Instr. and Meth.* **396**, p. 374, 1997.